PINDOC: Pedestrian Indoor Navigation System Integrating Deterministic, Opportunistic, and Cooperative Functionalities

Chi-Shih Jao, *Student Member, IEEE*, Ali A. Abdallah, *Student Member, IEEE*, Changwei Chen, Min-Won Seo, *Student Member, IEEE*, Solmaz S. Kia, *Senior Member, IEEE*, Zaher M. Kassas, *Senior Member, IEEE*, and Andrei M. Shkel, *Fellow, IEEE*

***Abstract*—In this paper, we present a Pedestrian Indoor Navigation system integrating Deterministic, Opportunistic, and Cooperative functionalities (PINDOC) for multi-agent navigation. The deterministic module produces a navigation solution for each agent by utilizing a Zero-velocity-UPdaTe (ZUPT)-aided Inertial Navigation System (INS) augmented with an altimeter and foot-to-foot range measurements. The opportunistic module augments the deterministic solutions with pseudorange measurements extracted from cellular Long-Term Evolution (LTE) signals. The navigation accuracy of each individual agent is further enhanced by cooperative localization using Ultra-WideBand (UWB)-based inter-agent range measurements. We developed a dedicated multi-sensor pedestrian navigation hardware testbed and conducted an experiment to evaluate the navigation performance of different combinations of components comprising PINDOC: ZUPT-aided INS, altimeter, foot-to-foot ranging, LTE signals, and inter-agent ranging. The experiment involved three agents, with one agent traversing a trajectory of 600 meters in 14 minutes, during which, the other two agents remained stationary. The traversed trajectory included terrains of flat surfaces, stairs, ramps, and elevators. The PINDOC system showed high accuracy, achieving a position Root-Mean-Squared Error (RMSE), maximum error, and final error of 0.93 m, 2.23 m, and 1.28 m over the 600-meter trajectory.**

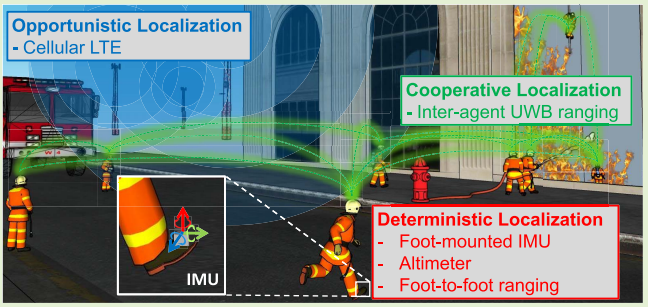

***Index Terms*—Indoor navigation, IMU, zero velocity update, inertial navigation, ultrasonic, barometer, foot-mounted IMU, beamforming, multipath mitigation, DNN, synthetic aperture, LTE, cooperative localization, UWB.**

I. Introduction

AN ACCURATE and reliable self-contained pedestrian indoor navigation system is essential for personnel safety in numerous applications, such as emergency response and military operations. Firefighters, first responders, and soldiers need to keep track of their locations all the time to plan escape and rescue strategies in extreme scenarios. In addition to degraded performance or failure of Global Navigation Satellite Systems (GNSS), these extreme scenarios often come with conditions where visibility is poor due to smoke or low light intensity and pre-installing dedicated infrastructure in the surrounding environment is often infeasible [1]. These conditions limit the use of many existing alternative navigation technologies, including Light Detection and Ranging (LiDAR) [2], Wi-Fi [3], Bluetooth [4], and cameras [5]–[8]. In such environments, a pedestrian navigation system using an Inertial Navigation System (INS) is preferable, because the system operates in a self-contained manner, requires no installation time, and produces measurements in a deterministic fashion [9]. Despite these attractive features, without an aiding source, the errors in an INS accumulate over time, causing the navigation solution to eventually drift unboundedly [10].

Pedestrian navigation systems using INS, or pedestrian INS, may have a number of different implementations [11]–[15]. Among these implementations, the system using foot-mounted Inertial Measurement Units (IMUs) has drawn attention for its ability to significantly enhance a strapdown INS using a

Manuscript received 20 May 2022; accepted 14 June 2022. Date of publication 22 June 2022; date of current version 14 July 2022. This work was supported by the U.S. Department of Commerce, National Institute of Standards and Technology (NIST), under Award 70NANB17H192. The associate editor coordinating the review of this article and approving it for publication was Prof. You Li. *(Corresponding author: Chi-Shih Jao.)*

Chi-Shih Jao, Changwei Chen, Min-Won Seo, Solmaz S. Kia, and Andrei M. Shkel are with the Department of Mechanical and Aerospace Engineering, University of California at Irvine, Irvine, CA 92697 USA (e-mail: chishihj@uci.edu; changwc3@uci.edu; minwons@uci.edu; solmaz@uci.edu; andrei.shkel@uci.edu).

Ali A. Abdallah is with the Department of Electrical Engineering and Computer Science, University of California at Irvine, Irvine, CA 92697 USA (e-mail: abdalla2@uci.edu).

Zaher M. Kassas is with the Department of Electrical Engineering and Computer Science and the Department of Mechanical and Aerospace Engineering, University of California at Irvine, Irvine, CA 92697 USA (e-mail: zkassas@ieee.org).

Digital Object Identifier 10.1109/JSEN.2022.3183887

Zero velocity UPdaTe (ZUPT) algorithm [16], [17]. Based on the assumption that velocities of a person's foot during walking are nearly equal to zero during the stance phase of a gait cycle, the ZUPT algorithm effectively reduces localization errors caused by noise and stochastic time-varying biases of IMUs in inertial navigation systems [18]. A standalone ZUPT-aided INS has been theoretically predicted and experimentally demonstrated to achieve an error of less than 1% of the traveling distance with an industrial-grade IMU [19]–[21].

Positioning accuracy of the ZUPT-aided Pedestrian INS has been reported to depend on several factors, and sensor fusion solutions have been popular approaches to improve the accuracy. The factors leading to position estimation errors include 1) noise characteristics of deployed IMUs, 2) performance of stance phase detection, 3) the unobservability of yaw angle estimation, and 4) unmodeled error that results from a violation of the assumption that the foot is completely stationary during the stance phase of a gait cycle [22], [23]. To overcome these challenges, self-contained aiding techniques based on other non-inertial sensors deployed on the same person for the ZUPT-aided INS have been developed. Different types of altimeters, such as barometric altimeters [24] and hybrid ultrasonic/barometric altimeters [25], that were collocated with a foot-mounted IMU, have been proven to bound position error growth along the vertical direction. To increase observability in the yaw angle estimation, mechanisms utilizing magnetometers [26], foot-to-foot ultrasonic sensors [27], [28], and foot-to-foot cameras [29] were developed. To increase the stance phase detection performance, downward-facing ultrasonic sensors [30], [31], Dynamic Vision Sensors (DVS) [32], pressure sensors [33], and permanent magnets [34] have been integrated with foot-mounted IMUs. The ZUPT-aided INS augmented by self-contained sensing modalities, which is collectively referred to as *deterministic localization* in this paper, was demonstrated to improve navigation accuracy, as compared to a standalone foot-mounted INS. However, absolute horizontal position uncertainties of the former systems propagate unboundedly and can eventually exceed desired localization accuracy in a long-term pedestrian navigation task.

To improve localization accuracy of the deterministic localization for long-term navigation tasks, infrastructure-free solutions using opportunistic exteroceptive external aiding signals have been explored. The prime examples are *Cooperative Localization* (CL) [35], [36] and localization using cellular signals [37], [38]. In CL, a group of communicating agents, use inter-agent relative measurements as a feedback to improve their localization accuracy of their local filter, e.g., Pedestrian INS [36], [39]. CL in pedestrian navigation can be implemented based on inter-agent range measurements obtained using different mechanisms, including computer vision or wireless radio signals [40]. Among these implementations, Ultra-WideBand (UWB)-based range measurements have attracted significant attention in indoor navigation because the sensor has high time resolution, wide bandwidth, and capability to work under Non-Line-Of-Sight (NLOS) conditions [36]. On the other hand, in an *opportunistic localization* framework, cellular towers are treated as beacons, and positioning can be achieved by trilaterating pseudorange measurements based on cellular signals [41]. Cellular signals possess several desirable characteristics for indoor localization: abundance, geometric diversity, high bandwidth, high carrier-to-noise ratio (C/N_0) in indoor conditions, and the fact that some of their downlink signals are free to use [42], [43]. Cooperative and signal-based localization approaches have been demonstrated to provide relative and absolute position compensations to the deterministic approaches [44]–[46]. However, investigations of the effects of the former two approaches on deterministic approaches were usually conducted separately. To the authors' knowledge, no previous work has developed a navigation solution integrating the three localization approaches for indoor navigation.

In this paper, we propose a Pedestrian Indoor Navigation system integrating Deterministic, Opportunistic, and Cooperative functionalities (PINDOC) for navigation of multiple agents. The proposed PINDOC can be implemented in different configurations, providing a navigation solution using a different combination of the deterministic, opportunistic, and cooperative functionalities. The deterministic approach utilizes dual foot-mounted IMUs and implements ZUPT-aided INS augmented by barometric altimeter and foot-to-foot range measurements. The opportunistic approach uses psuedorange measurements extracted from cellular Long-Term Evolution (LTE) towers and implements a Deep Neural Network (DNN)-based Synthetic Aperture Navigation (SAN) to spatially mitigate multipath. This approach operates in a base/rover framework in order to tackle one of the main challenges of LTE opportunistic navigation, i.e., the unknown cellular towers' clock states. The cooperative localization approach uses UWBs for inter-agent range measurements and differentiates Line-Of-Sight (LOS) and NLOS components using a power-metric-based detector. The proposed PINDOC is implemented with an Extended Kalman Filter (EKF) in a centralized manner. This paper makes the following contributions:

1) develops a multi-agent indoor navigation solution, PINDOC, that utilizes deterministic, opportunistic, and cooperative functionalities,
2) develops a dedicated pedestrian navigation testbed that integrates multiple sensors including IMUs, barometers, UWBs, and LTE receivers,
3) compares navigation accuracy of the developed systems implemented in different configurations using a real-world pedestrian indoor navigation experiment.

The rest of the paper is organized as follows. Section II presents the mathematical model of the proposed approach. Section III demonstrates a hardware system that realizes the proposed algorithm. Section IV discusses validation experiments. Section V presents concluding remarks.

II. The Proposed Approach

The proposed PINDOC system uses an EKF as the navigation filter. The proposed framework is illustrated in Fig. 1. In this section, we discuss the EKF framework that fuses

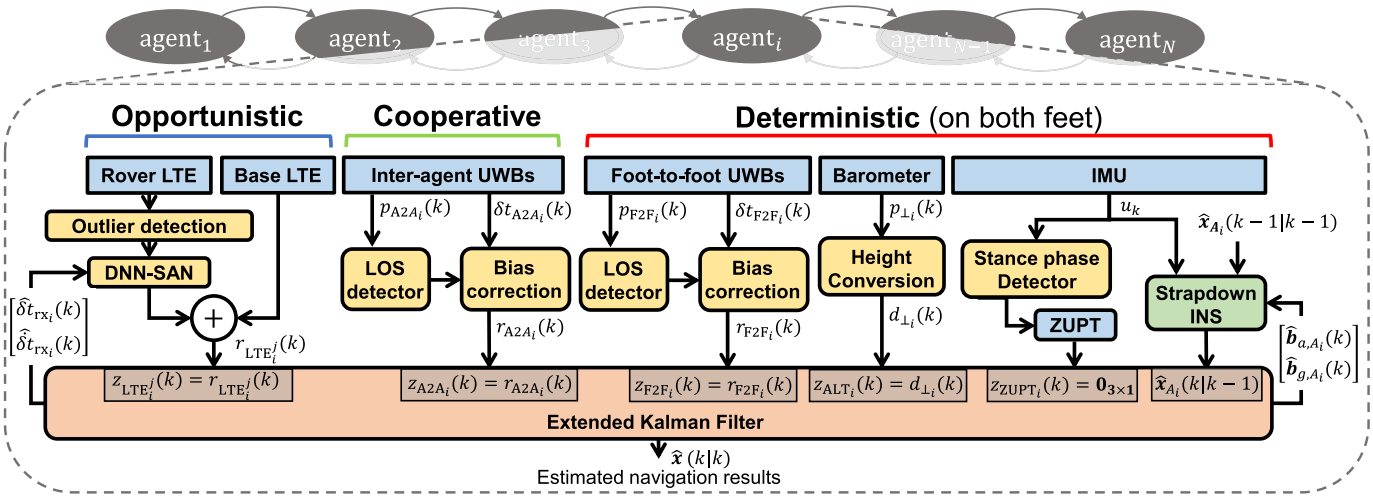

Fig. 1. Framework for the proposed pedestrian indoor navigation system integrating deterministic, opportunistic, and cooperative functionalities (PINDOC). The deterministic module produces navigation solutions for each agent with a zero-velocity-UPdaTe (ZUPT)-aided inertial navigation systems (INS) augmented with sensing modalities including altimeters and foot-to-foot range measurements. The opportunistic module enhances the deterministic solutions with pseudorange measurements collected based on cellular long-term evolution (LTE) signal of opportunity (SOP). Navigation accuracy of each individual agent is further enhanced by cooperative localization using UWB-based inter-agent range measurements.

the deterministic, opportunistic, and cooperative localization approaches used in the PINDOC.

The EKF estimates the state vector $\mathbf{x}(k)$ for a group of N agents, expressed as:

$$\mathbf{x}(k) = [\mathbf{x}_{\mathrm{A}_1}^\top(k), \mathbf{x}_{\mathrm{A}_2}^\top(k), \ldots, \mathbf{x}_{\mathrm{A}_N}^\top(k), \mathbf{x}_{\mathrm{LTE}_1}^\top(k), \mathbf{x}_{\mathrm{LTE}_2}^\top(k), \ldots, \mathbf{x}_{\mathrm{LTE}_N}^\top(k)]^\top,$$

where A_i denotes agent i in the group, and $\mathbf{x}_{\mathrm{A}_i}(k)$ and $\mathbf{x}_{\mathrm{LTE}_i}(k)$ are the states associated with agent i, described as

$$\begin{aligned}\mathbf{x}_{\mathrm{A}_i}(k) = [&\mathbf{q}_{\mathrm{A}_i^l}^\top(k), \mathbf{v}_{\mathrm{A}_i^l}^\top(k), \mathbf{p}_{\mathrm{A}_i^l}^\top(k), \mathbf{b}_{a,\mathrm{A}_i^l}^\top(k), \mathbf{b}_{g,\mathrm{A}_i^l}^\top(k),\\ &\mathbf{q}_{\mathrm{A}_i^r}^\top(k), \mathbf{v}_{\mathrm{A}_i^r}^\top(k), \mathbf{p}_{\mathrm{A}_i^r}^\top(k),\\ &\mathbf{b}_{a,\mathrm{A}_i^r}^\top(k), \mathbf{b}_{g,\mathrm{A}_i^r}^\top(k)]^\top \in \mathbb{R}^{30\times1},\\ \mathbf{x}_{\mathrm{LTE}_i}(k) = [&c\delta t_{\mathrm{rx}_i}(k), c\dot{\delta}t_{\mathrm{rx}_i}(k)]^\top \in \mathbb{R}^{2\times1},\end{aligned}$$

where $\mathbf{q}_{\mathrm{A}_i^l}(k), \mathbf{v}_{\mathrm{A}_i^l}(k), \mathbf{p}_{\mathrm{A}_i^l}(k), \mathbf{b}_{a,\mathrm{A}_i^l}(k)$, and $\mathbf{b}_{g,\mathrm{A}_i^l}(k)$ represent states of the left foot of agent i, including orientations, velocities, positions in the navigation frame, and accelerometer and gyroscope biases in the sensor body frame. $\mathbf{q}_{\mathrm{A}_i^r}(k), \mathbf{v}_{\mathrm{A}_i^r}(k), \mathbf{p}_{\mathrm{A}_i^r}(k), \mathbf{b}_{a,\mathrm{A}_i^r}(k)$, and $\mathbf{b}_{g,\mathrm{A}_i^r}(k)$ are the corresponded states of the right foot agent i. $c\delta t_{\mathrm{rx}_i}(k)$ and $c\dot{\delta}t_{\mathrm{rx}_i}(k)$ indicate the speed of light, c, multiplied by estimated clock bias and drift of an LTE receiver mounted on agent i. This expression of $\mathbf{x}_{\mathrm{LTE}_i}(k)$ has an unit of meter, which is beneficial for numerical calculations, as compared to directly using clock bias and drift.

A. Deterministic

The deterministic approach is used in the prediction step of the EKF and corrects the states in the update step with sensor measurements acquired from self-contained sensors mounted on the shoes of the same agent. The self-contained sensors include two sets of an IMU, an altimeter, and a UWB. One set of sensors is mounted on each foot of the agent.

1) Strapdown Inertial Navigation Systems: In the prediction step, the state propagation is implemented by inputting the IMU measurements on each foot to the strapdown inertial navigation systems [18]. The linearized state transition matrix corresponding to strapdown INS, denoted as $\mathbf{F}_{\mathrm{INS}}(k)$, is expressed as follows:

$$\mathbf{F}_{\mathrm{INS}}(k) = e^{\mathbf{A}_{\mathrm{INS}}(t_k)dt},$$

where dt is the sampling rate of the system and

$$\mathbf{A}_{\mathrm{INS}}(t) = \begin{bmatrix} \mathbf{A}_{\mathrm{A}_1}(t) & \mathbf{0}_{30\times30} & \cdots & \mathbf{0}_{30\times30} \\ \mathbf{0}_{30\times30} & \mathbf{A}_{\mathrm{A}_2}(t) & & \vdots \\ \vdots & & \ddots & \mathbf{0}_{30\times30} \\ \mathbf{0}_{30\times30} & \cdots & \mathbf{0}_{30\times30} & \mathbf{A}_{\mathrm{A}_N}(t) \end{bmatrix},$$

with

$$\mathbf{A}_{\mathrm{A}_i}(t) = \begin{bmatrix} \mathbf{A}_{\mathrm{A}_i^l}(t) & \mathbf{0}_{15\times15} \\ \mathbf{0}_{15\times15} & \mathbf{A}_{\mathrm{A}_i^r}(t) \end{bmatrix},$$

and

$$\mathbf{A}_{\mathrm{A}_i^l}(t) = \begin{bmatrix} \mathbf{0}_{3\times3} & \mathbf{0}_{3\times3} & \mathbf{0}_{3\times3} & -\mathrm{C}(\mathbf{q}_{\mathrm{A}_i^l}(k)) & \mathbf{0}_{3\times3} \\ [\overrightarrow{f_l}^n\times] & \mathbf{0}_{3\times3} & \mathbf{0}_{3\times3} & \mathbf{0}_{3\times3} & \mathrm{C}(\mathbf{q}_{\mathrm{A}_i^l}(k)) \\ \mathbf{0}_{3\times3} & \mathbf{I}_{3\times3} & \mathbf{0}_{3\times3} & \mathbf{0}_{3\times3} & \mathbf{0}_{3\times3} \\ \mathbf{0}_{3\times3} & \mathbf{0}_{3\times3} & \mathbf{0}_{3\times3} & \mathbf{0}_{3\times3} & \mathbf{0}_{3\times3} \\ \mathbf{0}_{3\times3} & \mathbf{0}_{3\times3} & \mathbf{0}_{3\times3} & \mathbf{0}_{3\times3} & \mathbf{0}_{3\times3} \end{bmatrix}.$$

Here, $[\overrightarrow{f_l}^n\times]$ is the skew-symmetric cross-product-operator of the accelerometer outputs of the left IMU, expressed in the navigation frame. $\mathrm{C}(\mathbf{q})$ is the Directional Cosine Matrix (DCM) corresponding to the quaternion vector $\mathbf{q}$. $\mathbf{0}_{n\times m}$ indicates a zero matrix having n number of rows and m number of columns. $\mathbf{A}_{\mathrm{A}_i^r}(t)$ is constructed in the same manner as $\mathbf{A}_{\mathrm{A}_i^l}(t)$ except that the states corresponding to the right foot are used.

The process noise matrix corresponding to strapdown INS, denoted as $\mathbf{Q}_{\text{INS}}(k)$, is expressed as

$$\mathbf{Q}_{\text{INS}}(k) = \begin{bmatrix} \mathbf{Q}_{\text{A}_1}(k) & \mathbf{0}_{30\times30} & \cdots & \mathbf{0}_{30\times30} \\ \mathbf{0}_{30\times30} & \mathbf{Q}_{\text{A}_2}(k) & & \vdots \\ \vdots & & \ddots & \mathbf{0}_{30\times30} \\ \mathbf{0}_{30\times30} & \cdots & \mathbf{0}_{30\times30} & \mathbf{Q}_{\text{A}_N}(k) \end{bmatrix},$$

$$\mathbf{Q}_{\text{A}_i}(k) = \begin{bmatrix} \mathbf{Q}_{\text{A}_i^l}(k) & \mathbf{0}_{15\times15} \\ \mathbf{0}_{15\times15} & \mathbf{Q}_{\text{A}_i^r}(k) \end{bmatrix},$$

with $\mathbf{Q}_{\text{A}_i^l}(k) =$

$$\begin{bmatrix} \sigma^2_{\text{ARW}}\mathbf{I}_{3\times3} & \mathbf{0}_{3\times3} & \mathbf{0}_{3\times3} & \mathbf{0}_{3\times3} & \mathbf{0}_{3\times3} \\ \mathbf{0}_{3\times3} & \sigma^2_{\text{VRW}}\mathbf{I}_{3\times3} & \mathbf{0}_{3\times3} & \mathbf{0}_{3\times3} & \mathbf{0}_{3\times3} \\ \mathbf{0}_{3\times3} & \mathbf{I}_{3\times3} & \mathbf{0}_{3\times3} & \mathbf{0}_{3\times3} & \mathbf{0}_{3\times3} \\ \mathbf{0}_{3\times3} & \mathbf{0}_{3\times3} & \mathbf{0}_{3\times3} & \sigma^2_{\text{AcRW}}\mathbf{I}_{3\times3} & \mathbf{0}_{3\times3} \\ \mathbf{0}_{3\times3} & \mathbf{0}_{3\times3} & \mathbf{0}_{3\times3} & \mathbf{0}_{3\times3} & \sigma^2_{\text{RRW}}\mathbf{I}_{3\times3} \end{bmatrix}.$$

Here, $\mathbf{I}_{n\times n}$ is the identity matrix having n number of rows and columns. $\sigma^2_{\text{ARW}_i}$, $\sigma^2_{\text{VRW}_i}$, $\sigma^2_{\text{RRW}_i}$, and $\sigma^2_{\text{AcRW}_i}$ are the Angle Random Walk of the gyroscopes, the Velocity Random Walk of the accelerometers, the Rate Angle Walk of the gyroscopes, and the Acceleration Random Walk of the accelerometers of the IMU mounted on the left shoe of agent i. In this paper, we set $\mathbf{Q}_{\text{A}_i^r}(k) = \mathbf{Q}_{\text{A}_i^l}(k)$ based on an assumption that two IMUs, each mounted on the same agent's left and right feet, have similar noise characteristics.

2) Zero Velocity Update: When a stance phase is detected, the ZUPT algorithm is activated to compensate for the velocity state in the update step of the EKF. The compensation is done by feeding in pseudo-measurements of zero velocity along the three axes, which is denoted as $\mathbf{v}_{\text{ZUPT}}(k) = \mathbf{0}_{3\times1}$. In this paper, the stance phase detection is achieved with the Stance Hypothesis Optimal dEtection (SHOE) detector [47]. For the states associated with the left and the right feet of agent i, the ZUPT measurement models, $\mathbf{z}_{\text{ZUPT}_i^l}(k)$ and $\mathbf{z}_{\text{ZUPT}_i^r}(k)$, measurement matrices, $\mathbf{H}_{\text{ZUPT}_i^l}(k)$ and $\mathbf{H}_{\text{ZUPT}_i^r}(k)$, and measurement covariance matrices, $\mathbf{R}_{\text{ZUPT}_i^l}(k)$ and $\mathbf{R}_{\text{ZUPT}_i^r}(k)$, are expressed as follows:

$$\mathbf{z}_{\text{ZUPT}_i^l}(k) = \mathbf{z}_{\text{ZUPT}_i^r}(k) = \mathbf{v}_{\text{ZUPT}}(k)$$

$$\mathbf{H}_{\text{ZUPT}_i^l}(k) = \begin{bmatrix} \mathbf{0}_{((i-1)\times30+3)\times3} \\ \mathbf{I}_{3\times3} \\ \mathbf{0}_{(24+(N-i)\times30+2N)\times3} \end{bmatrix}^\top$$

$$\mathbf{H}_{\text{ZUPT}_i^r}(k) = \begin{bmatrix} \mathbf{0}_{((i-1)\times30+18)\times3} \\ \mathbf{I}_{3\times3} \\ \mathbf{0}_{(9+(N-i)\times30+2N)\times3} \end{bmatrix}^\top$$

$$\mathbf{R}_{\text{ZUPT}_i^l}(k) = \mathbf{R}_{\text{ZUPT}_i^r}(k) = \sigma^2_{\text{ZUPT}_i}\mathbf{I}_{3\times3},$$

where $\sigma^2_{\text{ZUPT}_i}$ is the noise variance of the zero-velocity measurement $\mathbf{v}_{\text{ZUPT}}$ for agent i.

3) Altimeter Measurements: In pedestrian navigation, altitude measurements can be obtained from a barometer [24] or, in a hybrid approach, using both barometer and ultrasonic sensors [25]. At time k, altimeters mounted on the left and the right shoes of agent i provide measurements of vertical displacements in the navigation frame, which are denoted as $d_{\perp_i^l}(k)$ and $d_{\perp_i^r}(k)$, respectively. The altimeter measurements are used in the update step of the EKF to bound error growth of estimated position along the vertical direction [24]. The measurement models corresponding to the altimeter on the left and right feet of agent i, $z_{\text{ALT}_i^l}(k)$ and $z_{\text{ALT}_i^r}(k)$, are described as follows:

$$z_{\text{ALT}_i^l}(k) = d_{\perp_i^l}(k), z_{\text{ALT}_i^r}(k) = d_{\perp_i^r}(k).$$

The associated measurement matrices are described as

$$\mathbf{H}_{\text{ALT}_i^l}(k) = \left[\mathbf{0}_{1\times((i-1)\times30+8)}\ 1\ \mathbf{0}_{1\times(21+(N-i)\times30+2N)}\right]$$
$$\mathbf{H}_{\text{ALT}_i^r}(k) = \left[\mathbf{0}_{1\times((i-1)\times30+23)}\ 1\ \mathbf{0}_{1\times(6+(N-i)\times30+2N)}\right].$$

The measurement noise covariance matrices are described as

$$\mathbf{R}_{\text{ALT}_i^l}(k) = \mathbf{R}_{\text{ALT}_i^r}(k) = \sigma^2_{\text{ALT}_i},$$

where $\sigma^2_{\text{ALT}_i}$ is the noise variance of the altimeter measurements for agent i.

4) Foot-to-Foot Ranging Measurements: Distance measurements between the two feet of agent i, denoted as $r_{\text{F2F}_i}(k)$, can be obtained from various different sensing modalities, including ultrasonic sensors [28], foot-to-foot cameras [29], electromagnetic systems [20], and UWB [48], [49]. In this paper, UWB-based foot-to-foot ranging measurements are used. The foot-to-foot range measurements are classified into LOS and NLOS by a power metric-based approach [36]. In this paper, only LOS UWB measurements are used. The range measurements are processed with bias correction. The processed foot-to-foot measurements are fused in the update step of the EKF to compensate for relative distances between the two feet [27]. The corresponding measurement model, $z_{\text{F2F}_i}(k)$, and measurement matrix, $\mathbf{H}_{\text{F2F}_i}(k)$, are described as follows:

$$z_{\text{F2F}_i}(k) = r_{\text{F2F}_i}(k)$$

$$\mathbf{H}_{\text{F2F}_i}(k) = \begin{bmatrix} \mathbf{0}_{((i-1)\times30+6)\times1} \\ \frac{\partial\|\mathbf{p}_{\text{A}_i^l}(k)-\mathbf{p}_{\text{A}_i^r}(k)\|^\top}{\partial\mathbf{p}_{\text{A}_i^l}} \\ \mathbf{0}_{15\times1} \\ \frac{\partial\|\mathbf{p}_{\text{A}_i^l(k)}-\mathbf{p}_{\text{A}_i^r}(k)\|^\top}{\partial\mathbf{p}_{\text{A}_i^r}(k)} \\ \mathbf{0}_{(6+(N-i)\times30+2N)\times1} \end{bmatrix}^\top.$$

The measurement noise covariance matrices are described as

$$\mathbf{R}_{\text{F2F}_i}(k) = \sigma^2_{\text{F2F}_i},$$

where $\sigma^2_{\text{F2F}_i}$ is the noise variance of the foot-to-foot range measurements for agent i.

B. Cooperative

The CL approach is realized through inter-agent ranging measurements obtained from UWB sensors attached to the right shoe of each agent. Similar to the foot-to-foot range measurements, the measurements between agent i and agent h, denoted as $r_{\text{A2A}_i^h}(k)$, are classified into LOS and NLOS

cases, and only LOS cases are used in the update step of the EKF. The LOS measurements are further processed with bias correction. Assuming that $i < h$, the corresponding inter-agent range measurement model, $z_{\mathrm{A2A}_i^h}(k)$, and measurement matrix, $\mathbf{H}_{\mathrm{F2F}_i^h}(k)$, are described as follows:

$$z_{\mathrm{A2A}_i^h}(k) = r_{\mathrm{A2A}_i^h}(k)$$

$$\mathbf{H}_{\mathrm{A2A}_i^h}(k) = \begin{bmatrix} \mathbf{0}_{((i-1)\times 30+21)\times 1} \\ \frac{\partial ||\mathbf{p}_{\mathrm{A}_i^r}(k) - \mathbf{p}_{\mathrm{A}_h^r}(k)||^\top}{\partial \mathbf{p}_{\mathrm{A}_i^r}(k)} \\ \mathbf{0}_{(6+(h-i-1)\times 30+21)\times 1} \\ \frac{\partial ||\mathbf{p}_{\mathrm{A}_i^r,k} - \mathbf{p}_{\mathrm{A}_h^r,k}||^\top}{\partial \mathbf{p}_{\mathrm{A}_h^r,k}} \\ \mathbf{0}_{(6+(N-h)\times 30+2N)\times 1} \end{bmatrix}^\top.$$

The measurement noise covariance matrices are described as

$$\mathbf{R}_{\mathrm{A2A}_i^h}(k) = \sigma^2_{\mathrm{A2A}_i^h},$$

where $\sigma^2_{\mathrm{A2A}_i^h}$ is the noise variance of the inter-agent range measurements between agent i and agent h.

C. Opportunistic

In the proposed framework, cellular LTE signals are utilized to provide absolute positioning measurements. This is achieved by exploiting LTE downlink signals opportunistically in a base/rover LTE-DNN-SAN framework. In the proposed framework, a "base" LTE receiver is located outside the building and has access to GNSS signals. The base collects signals from multiple LTE towers (also known as eNodeBs) in the environment. The positions of the eNodeBs are pre-surveyed and assumed to be known (e.g., according to [50]). The base receiver estimates the eNodeBs' clock biases and shares this information with the indoor receivers denoted by "rovers." Each rover has a copy of the same LTE receiver used in the base unit; however, a DNN-based SAN correction block is applied, in which the pedestrian's motion is utilized to synthesize a geometrically-separated antenna array from time-separated snapshots. This allows for beamforming towards the LOS from the rover to the LTE eNodeB, while suppressing multipath components. This process requires obtaining the LOS steering vector, which is obtained by taking the nearest direction-of-arrival (DOA) estimate from the proposed DNN-DOA estimator to the LOS DOA estimated using the current estimate of the rover's position and the known LTE eNodeB positions. Fig. 2 depicts the block diagram of the LTE-DNN-SAN framework. Further details can be found in [51].

The EKF prediction step propagates the state $\mathbf{x}_{\mathrm{LTE}_i}(k)$ with following state transition matrix $\mathbf{F}_{\mathrm{LTE}_i}(k)$ and process noise covariance $\mathbf{Q}_{\mathrm{LTE}_i}(k)$

$$\mathbf{F}_{\mathrm{LTE}_i}(k) = = \begin{bmatrix} 1 & dt \\ 0 & 1 \end{bmatrix}$$

$$\mathbf{Q}_{\mathrm{LTE}_i}(k) = c^2 \begin{bmatrix} \sigma_{\delta t_{rx_i}} dt + \sigma_{\dot{\delta} t_{rx_i}} \frac{dt^3}{3} & \sigma_{\dot{\delta} t_{rx_i}} \frac{dt^2}{2} \\ \sigma_{\dot{\delta} t_{rx_i}} \frac{dt^2}{2} & \sigma_{\dot{\delta} t_{rx_i}} dt \end{bmatrix},$$

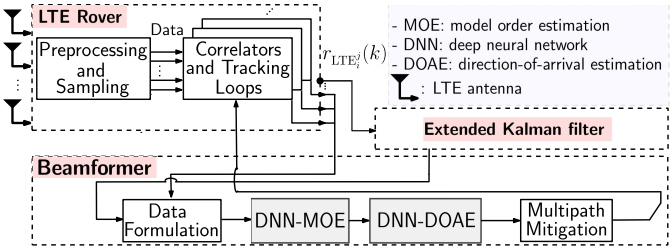

Fig. 2. A block diagram depicting the LTE-DNN-SAN block diagram used in the proposed PINDOC framework shown in Fig. 1.

where $\sigma_{\delta t_{rx_i}}$ and $\sigma_{\dot{\delta} t_{rx_i}}$ are parameters associated with clock quality. Details regarding modeling of the clock bias and drift are documented in [43].

In the update step of the EKF, LTE psuedorange measurements are fused in a tightly-coupled manner with the deterministic and the cooperative approaches. For LTE signals that are transmitted from eNodeB j and received by LTE receiver on agent i, the associated pseudorange measurement is denoted as $r_{\mathrm{LTE}_i^j}(k)$. The location of eNodeB j is represented by $\mathbf{p}_{\mathrm{eNodeB}_j}$. The corresponding measurement model, $z_{\mathrm{LTE}_i^j}(k)$, measurement matrix, $\mathbf{H}_{\mathrm{LTE}_i^j}(k)$, and measurement covariance matrix, $\mathbf{R}_{\mathrm{LTE}_i^j}(k)$, are described as follows:

$$z_{\mathrm{LTE}_i^j}(k) = r_{\mathrm{LTE}_i^j}(k)$$

$$\mathbf{H}_{\mathrm{LTE}_i^j}(k) = \begin{bmatrix} \mathbf{0}_{((i-1)\times 30+21)\times 1} \\ \frac{\partial ||\mathbf{p}_{\mathrm{A}_i^r}(k) - \mathbf{p}_{\mathrm{eNodeB}_j}||^\top}{\partial \mathbf{p}_{\mathrm{A}_i^r}(k)} \\ \mathbf{0}_{(6+(N-i)\times 30)\times 1} \\ \mathbf{0}_{((i-1)\times 2)\times 1} \\ 1 \\ \mathbf{0}_{(1+(N-i)\times 2)\times 1} \end{bmatrix}^\top$$

$$\mathbf{R}_{\mathrm{LTE}_i^j}(k) = \sigma^2_{\mathrm{LTE}_i^j}.$$

Here, $\sigma^2_{\mathrm{LTE}_i^j}$ is an adaptive value based on $c^2 \frac{\alpha}{(C/N_0)_i^j}$, where $(C/N_0)_i^j$ is the signal-to-noise ratios of the pseudorange measurement $r_{\mathrm{LTE}_i^j}(k)$ and α is a tuning parameter that was chosen to be 2.22×10^{-11} [43]. To detect and remove outliers from LTE observables, a rudimentary innovation-based detector is implemented to filter out inconsistent LTE observables [52].

D. The EKF for PINDOC

The proposed PINDOC combines the deterministic, opportunistic, and cooperative localization approaches in the EKF. When each of the sensing modalities mentioned previously becomes available, the EKF stacks all available measurements and performs the update step. Settings of the noise parameters are determined based on noise characteristics of sensors involved in the implementation.

III. System Hardware

In this section, we discuss experimental hardware, shown in Fig. 3, that is designed to evaluate navigation performance of the proposed PINDOC.

A. Lab-On-Shoe Platform

The Lab-On-Shoe platform, shown in Fig. 3, is responsible for acquisition of all sensor measurements, except for foot-to-foot ranges, that are associated with the deterministic localization. The Lab-On-Shoe was developed in Microsystems Lab at the University of California, Irvine, as a reconfigurable multi-sensor pedestrian navigation testbed [53]. The agent wears the Lab-On-Shoe platform on both left and right feet. Each shoe of the platform includes an Analog Device ADIS16497-3 tactical-grade IMU, an MS5803-01BA barometric altimeter, an SRF08 ultrasonic sensor, and two SRF02 ultrasonic sensors. The barometer has a nominal resolution of 10 cm in vertical displacement measurement, and the ultrasonic sensor has a range resolution of 1 cm. In this paper, the ultrasonic sensors were not used in the experiment discussed in Section IV. A microcontroller Teensy 3.2 is used to implement digital communication protocols, including the Inter-Integrated Circuit (I^2C) and Serial Peripheral Interface (SPI), to collect sensor measurements on the Lab-On-Shoe platform. The sampling rate of IMUs and altimeters are 1000 Hz and 20 Hz, respectively. The collected measurements are transmitted to a laptop with the Universal Asynchronous Receiver-Transmitter (UART) through a USB cable for data logging.

B. LTE Receivers and Processing Modules

LTE signals are used to realize the opportunistic approach for the proposed PINDOC. Each agent in the PINDOC carries a backpack where an LTE receiver is mounted and contains an LTE receiver, a laptop, a battery, and a storage hard drive. The LTE receiver, developed at the Autonomous Systems Perception, Intelligence, & Navigation (ASPIN) Laboratory [43], is equipped with four consumer-grade cellular omni-directional Laird antennas, and a quad-channel National Instruments (NI) Universal Software Radio Peripheral (USRP)-2955 is used to simultaneously down-mix and synchronously sample LTE signals at 10 Megasamples per second (Msps). The sampled LTE signals are transferred from the USRP-2955 via a PCI Express cable and stored on a laptop for post-processing. The LTE measurements have a sampling rate of 100 Hz.

C. Cooperative Module

One cooperative module, shown in Fig. 3, is mounted on each shoe of the Lab-On-Shoe platform. Each of the modules includes a UWB DWM1000, a microcontroller Teensy 3.2, a Bluetooth device HC-05, and a lithium battery [54]. The microcontroller running at a clock rate of 120 Mhz implements an SPI protocol to communicate with the UWB, and the battery provides a power source for the entire module. The module on the left shoe of an agent is paired up with the modules located on the right foot of all other agents and obtains three pieces of information: range, power metric (PM), and agent identification (ID). PM is the difference between the total received signal power and the direct-path signal power and is used for LOS/NLOS detection. The range measurements are used for foot-to-foot ranging when obtained from two UWBs mounted on the same agent and for inter-agent ranging

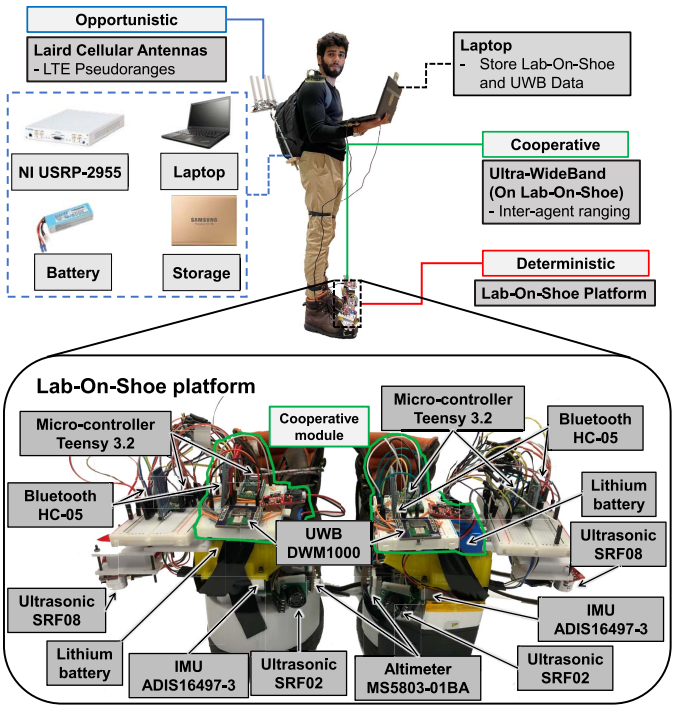

Fig. 3. Experimental setup used for investigation of the navigation performance of the proposed PINDOC. The deterministic localization approach was realized with the lab-on-shoe platform, which integrated sensing modalities including IMUs, altimeters, and ultrasonic sensors. In this paper, only IMU and altimeters were used. The opportunistic LTE-based pseudoranges were collected by the Laird cellular antennas and their corresponding signal processing units. The cooperative modules mounted on the lab-on-shoe platform included UWBs for foot-to-foot ranging and inter-agent ranging measurements. The laptop was used in the experiment for data logging.

when collected from the sensors mounted on two different agents. The collected measurements, including range, PM, and agent ID, are transmitted to nearby Teensy 3.2 on the Lab-On-Shoe platform in UART communication protocol via the Bluetooth transmitter. The sampling rate of the UWB range measurements is 10 Hz.

The developed pedestrian navigation testbed shown in Fig. 3 was designed as a research prototype to quickly and flexibly investigate different localization accuracy of algorithms for pedestrian indoor navigation systems. In Fig. 3, the hardware mounted on each shoe of the Lab-On-Shoe systems, the LTE backpack, and handheld laptop weighted 237 g, 5.44 kg, and 1.53 kg, respectively. It has been demonstrated that it is possible to adapt this pedestrian navigation testbed into a minimized wearable device for practical, real-life applications. For the deterministic module, foot-mounted IMU systems, such as the Sugar-Cube platform [31] and the OpenShoe module [55], with small form factors and real-time positioning functionality have been developed; For the cooperative module, systems like the TRX system [56] are commercially available. For the opportunistic module, it can be implemented on a modern smartphone with the limitation of the number of available RF Front-Ends and the available resources from the cellular modem. For implementing the full capability of opportunistic navigation, hardware (i.e., cellular modem) modifications will be required.

TABLE I
LTE ENODEBS' CHARACTESTICS

eNodeB	Carrier frequency [MHz]	N_{ID}^{Cell}	Bandwidth [MHz]	Cellular provider
1	2125	223	20	Verizon
2	1955	11	20	AT&T
3	2145	441	20	T-Mobile
4	2112.5	401	20	AT&T

TABLE II
PARAMETERS FOR THE EKF

Hyper-parameter	Value
σ_{ARW_1}	2.7221×10^{-5}
σ_{VRW_1}	0.0017
σ_{RRW_1}	8.3174×10^{-7}
σ_{AcRW_1}	6.63×10^{-6}
σ_{ZUPT_1}	0.02
σ_{ALT_1}	0.1
σ_{F2F_1}	0.1
σ_{A2A_1}	1
σ_{LTE_1}	$\sqrt{c^2 \frac{2.22\times10^{-11}}{(C/N_0)}}$
$\sigma_{\delta t_{rx_i}}$	1.3×10^{-22}
$\dot{\sigma}_{\delta t_{rx_i}}$	7.8957×10^{-25}

IV. EXPERIMENT VALIDATION

To evaluate navigation performance of the proposed PINDOC, we conducted a pedestrian navigation experiment in an indoor environment at the Engineering Gateway Building at the University of California, Irvine. In this section, we describe the experiment, present our experimental results, and discuss the performance of the PINDOC.

A. Experiment Descriptions

The experiment involved three agents. Agent No.1, shown in Fig. 3, was equipped with the deterministic, opportunistic, and cooperative hardware. Agent No.2 and agent No.3 were both equipped with a set of the cooperative module. Figure 4(a) illustrates the experimental scenario, which is presented with point cloud points collected with a LiDAR module and cameras installed in an iPhone 12 Max. At the beginning of the experiment, agent No.1 stood outside of the first floor of the building for one minute to initialize the system. The GNSS and the altimeter mounted on agent No.1 obtained the initial position in latitude, longitude, and altitude during this period. The LTE receiver was initialized and started to track signals transmitted from four eNodeBs. The eNodeBs' characteristics are summarized in Table I. In the initialization process, accelerometer and gyroscope biases of the IMUs were calibrated. Noise parameters used in the EKF for PINDOC are listed in Table II.

After the initialization step, agent No.1 walked inside the building with a trajectory represented by the blue and the red curves in Fig. 4(b). The trajectory of the experiment included flat planes, stairs, ramps, and elevators. The length of the path was around 600 meters, and the duration was approximately 14 minutes. During the experiment, agent No.1 passed by the checkpoints marked with the green triangles in Fig. 4(b). The locations of the checkpoints were measured with an industrial ruler. The experiment was recorded using a smartphone camera, and the timestamps at which the agent passed through each checkpoint were visually determined from the video. During the entire experiment, agent No.2 and agent No.3 remained stationary at the location marked by the red and blue star markers in Fig. 4(b). The UWB sensors mounted on the right shoe of agent No.1 had an LOS connection with agent No.2 from 250 s to 310 s and with agent No.3 from 430 s to 485 s. Communication was lost in other periods of time because the UWB modules were too far apart and due to obstacles between the UWB modules. The measurements collected in this experiment indicate that the maximum communication range for the UWBs was around 30 m when there was a clear path for signals to be transmitted.

B. Performance Metrics

We considered seven performance metrics, including one computational complexity metric and six different accuracy metrics, to evaluate the navigation performance of the PINDOC. These metrics, listed in Table III, are processing time, position Root-Mean-Square Error (RMSE), two-dimensional (2D) RMSE, vertical ($\perp$) RMSE, position error Standard Deviation (SD), maximum displacement error, and final position error. In this paper, we used processing time to evaluate the computational complexity of a localization solution. The processing time is calculated based on the amount of time for the 2021a MATLAB program, operating on a laptop with an AMD Ryzen 9 5900HS Central Processing Unit (CPU) running at a clock rate of around 4 GHz, to compute a navigation solution based on collected sensor measurements.

The six accuracy metrics were chosen so that the navigation performance of the proposed PINDOC can be conveniently compared with the localization accuracy of other indoor navigation systems proposed in the literature. Among these six metrics, RMSE is often used to evaluate an estimated localization solution when reference trajectories along the three dimensions are available. 2D RMSE and $\perp$ RMSE are used as benchmarks when estimated positioning solutions emphasize accuracy in the horizontal and the vertical directions, respectively. Position error SD is used to quantify variations of displacement error. Maximum displacement error is used to investigate the worst-case scenarios of an estimated position. Finally, final position error is often used to evaluate dead-reckoning systems, which have localization errors accumulating with time, in navigation experiments where obtaining reference trajectories is challenging. For example, in many pedestrian navigation experiments involving using foot-mounted IMUs [38], the trajectories could cover large indoor areas, on the order of 50-100 m, and include a combination of complex terrains, such as flat planes, stairs, ramps, ladders, and elevators. Deploying a high-precision position reference system like the Opti-Track [57] or the Vicon [58] in such environments can be very expensive, and therefore, final position errors are used in these scenarios.

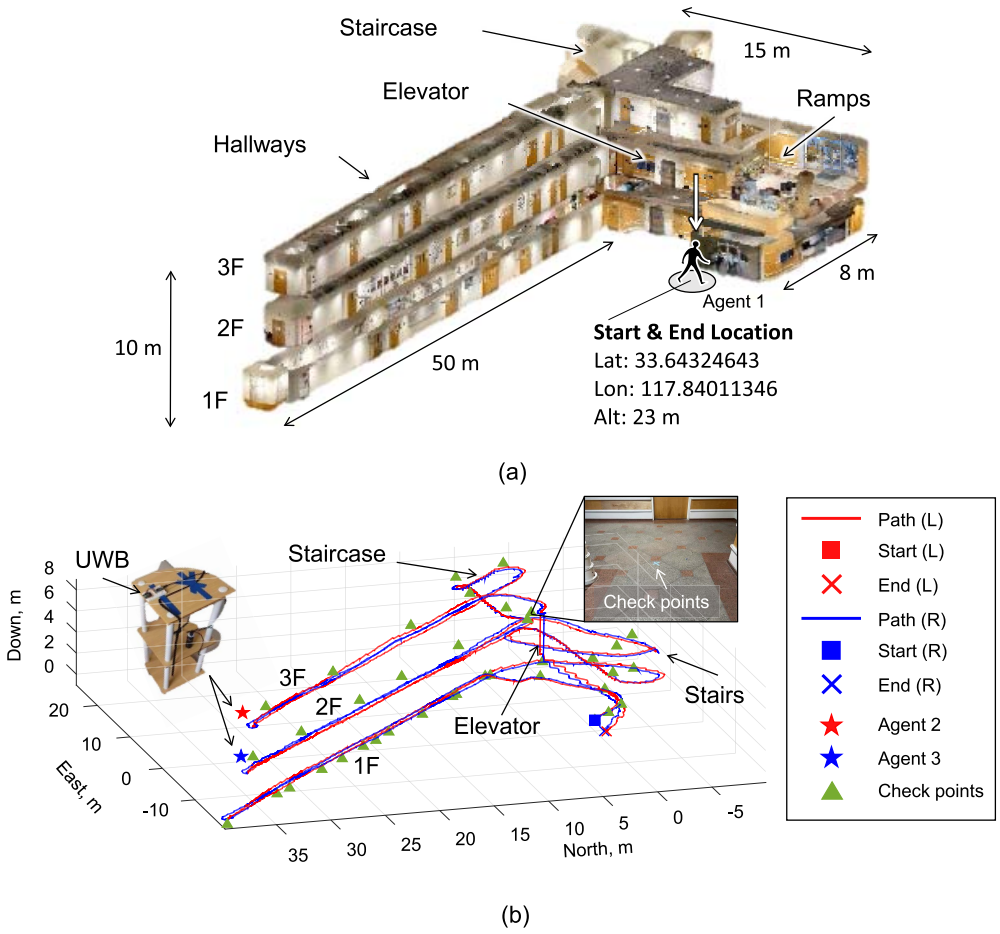

Fig. 4. (a) Point cloud map of the experimental scenario generated with LiDAR and camera modules installed on iPhone 12 max pro. (b) The blue and the red curves represent navigation solutions of the two feet of agent No.1 estimated by the proposed PINDOC implementing the ZUPT-aided INS augmented by altimeters, foot-to-foot ranging, and inter-agent ranging measurements in the experiment discussed in section IV. The blue star and the red star marked the locations of stationary agent No.2 and agent No.3 in the navigation frame. The green triangles represent checkpoints that were used to evaluate the in-trajectory localization performance of the navigation solutions.

TABLE III
NAVIGATION PERFORMANCE OF THE PROPOSED PINDOC IMPLEMENTED IN DIFFERENT CONFIGURATIONS

Config.	INS Aiding Method						Processing Time (s)	RMSE [m]	2D RMSE [m]	⊥ RMSE [m]	SD [m]	Max Error [m]	Final Error [m]
	ZUPT	ALT	F2F	A2	A3	LTE							
G	✓	✓	✓	✓	✓	✓	231.7	0.93	0.69	0.62	0.44	2.23	1.28
F	✓	✓	✓	✓	✓		211.6	0.93	0.69	0.62	0.44	2.23	1.32
D	✓	✓	✓	✓			211.0	0.94	0.71	0.62	0.43	2.23	1.32
E	✓	✓	✓		✓		210.9	0.95	0.72	0.62	0.46	2.23	1.68
I	✓	✓	✓			✓	227.0	0.96	0.74	0.62	0.45	2.23	1.64
C	✓	✓	✓				210.3	0.97	0.75	0.62	0.46	2.23	1.76
J	✓	✓				✓	234.0	1.07	0.87	0.62	0.48	2.44	1.51
B	✓	✓					207.4	1.64	1.52	0.59	0.75	2.9	2.55
K		✓				✓	227.9	1.97	1.65	0.67	0.88	7.74	3.2
H	✓					✓	222.0	2.48	0.90	2.32	1.87	10.02	10.02
A	✓						191.5	2.53	0.49	2.48	1.9	10.3	10.3

C. Experimental Results

This section compares the navigation performance for agent No.1 using the proposed PINDOC implemented in different configurations. Different configurations of the PINDOC use the ZUPT-aided INS, augmented by different combinations of various sensing modalities, namely altimeter (ALT), foot-to-foot ranging (F2F), inter-agent ranging with agent No.2 (A2) and agent No.3 (A3), and cellular LTE pseudo-range measurements. Trajectories estimated by the different configurations are presented in Fig. 5.

To quantify the localization error at each checkpoint for each navigation solution, we used the seven performance

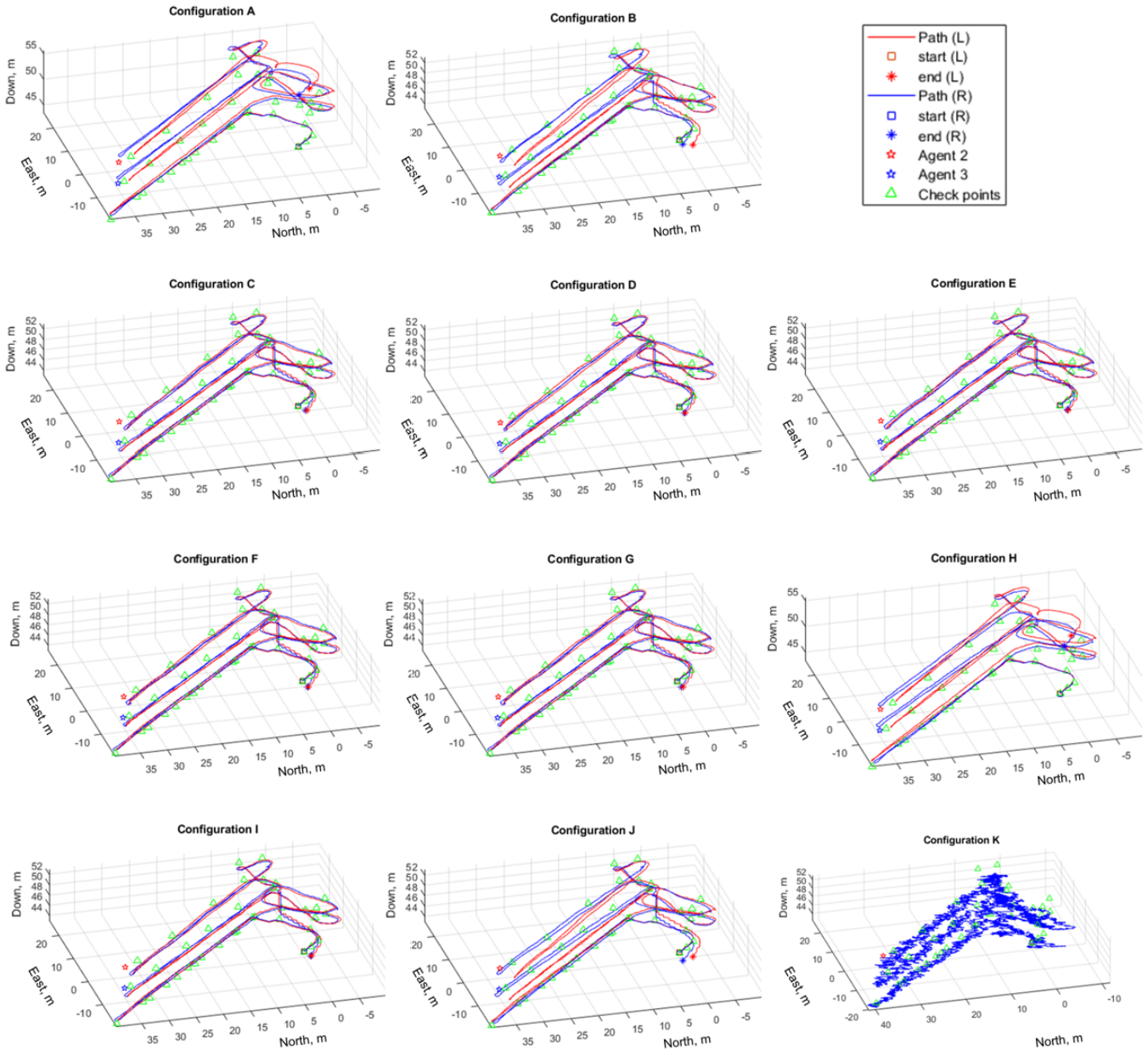

Fig. 5. Navigation trajectories estimated by different configurations of the proposed PINDOC. In the plot of configuration K, only the trajectory associated with Agent 1's right foot was shown because, in the experiment, only the navigation solution of the right foot was augmented with LTE pseudoranges. Error metrics of each of the configurations are documented in TABLE III.

metrics discussed in Section IV-B. Table III summarizes the performance of the navigation solutions using the PINDOC implemented in different configurations. The accuracy values presented in Table III were calculated based on the 38 checkpoints marked by the green triangles in Fig. 4. For the configurations where foot-to-foot ranging measurements were not involved, the accuracy metrics were calculated based on solutions of agent No.1's right foot as inter-agent range measurements were collected with the UWB module mounted on the right foot. The top item Table III, which is PINDOC with configuration G that uses ZUPT-aided INS augmented by ALT, F2F, A2, A3, and LTE had the smallest RMSE of 0.93 m. The bottom item in Table III, which is PINDOC with configuration A, had the largest RMSE of 2.53 m.

D. Discussion

The following remarks can be concluded from Table III.

- We could observe that enhancing the ZUPT-aided INS with more aiding methods led to better navigation accuracy, however, with a trade-off of increasing computational complexity. The smallest displacement error was achieved with configuration G, which uses the INS aided by the ZUPT algorithm, altimeter, foot-to-foot ranging measurements, the inter-agent range measurements from the other two agents, and LTE pseudorange measurements.
- It could be observed that the maximum position errors did not always occur at the end of the experiment. This could

be because, for dead reckoning systems, estimation errors on trajectory length get canceled out at return-to-home or loop-closure positions.

- In the configurations involving the LTE module, an innovation-based outlier detection module, as discussed in Section II-C, was used to produce the opportunistic navigation solutions. The outlier detection module detected if the LTE signal had large biases caused by the multi-path effect. In the case of a positive detection, the LTE psuedorange measurement was not used to augment the navigation solutions. It is worth mentioning that, in the experiment, we observed that the outlier detection module indicated several positive detections, and therefore, not all the LTE signals collected during the experiment were used in configuration G, H, I, and J. Nevertheless, when the outlier detection module showed negative detections, the opportunistic solution provided compensation for absolute position errors, increasing navigation accuracy.
- Configuration D and configuration E used deterministic solutions enhanced by inter-agent measurements from only one agent, but the former configuration had a smaller final displacement error. We considered the difference as a result of the experimental setup that agent No.1 first passed by agent No.3 and then agent No.2. This setup led to an advantage of configuration D that the position estimates were corrected by the stationary agent at a later time, and therefore, the final position estimated by configuration D had a smaller error than configuration E.
- In the cases of configurations A and H, where altimeter measurements were not used, the final position errors are much larger than in the other configurations. For configuration A, the final error is larger because when operating in the moving elevator, the stance phase detector used in the ZUPT algorithm would indicate that it is the stance phase and correct the velocity to zero, while in reality, the altitude of the agent was changing. In configuration H, we could see that augmenting the ZUPT-aided INS with LTE measurements could reduce the error. However, the horizontal distance between the receiver is significantly larger than the altitude of the LTE towers. As such, the agent's cellular-based navigation solution Vertical Dilution Of Precision (VDOP) will be large. Yet, LTE reduced the vertical errors slightly compared to standalone ZUPT.
- In the proposed PINDOC, aiding from LTE pseudorange measurements aims to compensate for absolute position errors. In the presented experiment with a duration of 14 min and a trajectory length of 600 m, the position errors in systems using only the deterministic and cooperative approaches have not grown to large values. Therefore, the compensation of errors provided by LTE signals was not significant. However, it is expected that in navigation experiments with a longer duration, the LTE module will play a significant role in bounding the position error growth of PINDOC and improving navigation accuracy.

V. Conclusion

In this paper, we proposed the PINDOC, which is a multi-agent pedestrian navigation system integrating the deterministic, the opportunistic, and the cooperative functionalities. The deterministic module uses sensing modalities, including IMUs, altimeters, and foot-to-foot range measurements. The opportunistic module utilizes cellular LTE pseudorange measurements, corrects clock biases with a base/rover framework, and mitigates multipath effect by DNN-SAN. The cooperative module enhances the navigation accuracy of each agent with UWB-based inter-agent range measurements. We developed a dedicated multi-sensor hardware platform and conducted an experiment with the platform to evaluate the navigation performance of the proposed PINDOC. The experiment was a 14-min and 600-m indoor pedestrian navigation task involving three agents, two of which were stationary and one of which was walking on terrains of flat surfaces, stairs, ramps, and elevators. We compared navigation accuracy using different configurations of the PINDOC for the moving agent. The experimental results showed that the configuration using ZUPT-aided INS enhanced by altimeters, foot-to-foot ranging, inter-agent ranging from the other two agents, and LTE pseudoranges had an position RMSE of 0.93 m and a position error SD of 0.44 m, which are the best navigation accuracy, as compared to other configurations of the proposed PINDOC. We conclude that the proposed PINDOC had a navigation error of less than 1 meter in terms of position RMSE in the experiment.

Acknowledgment

The authors would like to thank Jeb Benson, Former Technical Program Manager at NIST Public Safety Communication Research (PSCR), and Joseph Grasso, Portfolio Lead at PSCR Location-Based Services (LBS), for useful discussions. The content of this article is solely the responsibility of the authors and does not necessarily represent the official views of NIST.

References

[1] C. Fischer and H. Gellersen, "Location and navigation support for emergency responders: A survey," *IEEE Pervasive Comput.*, vol. 9, no. 1, pp. 38–47, Jan. 2010.

[2] G. A. Kumar, A. K. Patil, R. Patil, S. S. Park, and Y. H. Chai, "A LiDAR and IMU integrated indoor navigation system for UAVs and its application in real-time pipeline classification," *Sensors*, vol. 17, no. 6, p. 1268, 2017.

[3] Y. Shu *et al.*, "Gradient-based fingerprinting for indoor localization and tracking," *IEEE Trans. Ind. Electron.*, vol. 63, no. 4, pp. 2424–2433, Apr. 2015.

[4] Y. Zhuang, J. Yang, Y. Li, L. Qi, and N. El-Sheimy, "Smartphone-based indoor localization with Bluetooth low energy beacons," *Sensors*, vol. 16, no. 5, p. 596, Apr. 2016.

[5] T. Lemaire, C. Berger, I.-K. Jung, and S. Lacroix, "Vision-based SLAM: Stereo and monocular approaches," *Int. J. Comput. Vis.*, vol. 74, no. 3, pp. 343–364, Jul. 2007.

[6] F. Endres, J. Hess, N. Engelhard, J. Sturm, D. Cremers, and W. Burgard, "An evaluation of the RGB-D SLAM system," in *Proc. IEEE Int. Conf. Robot. Autom.*, May 2012, pp. 1691–1696.

[7] A. R. Vidal, H. Rebecq, T. Horstschaefer, and D. Scaramuzza, "Ultimate SLAM? Combining events, images, and IMU for robust visual SLAM in HDR and high-speed scenarios," *IEEE Robot. Autom. Lett.*, vol. 3, no. 2, pp. 994–1001, Apr. 2018.

[8] J. Fuentes-Pacheco, J. Ruiz-Ascencio, and J. M. Rendón-Mancha, "Visual simultaneous localization and mapping: A survey," *Artif. Intell. Rev.*, vol. 43, no. 1, pp. 55–81, 2015.

[9] P. Barsocchi, S. Chessa, F. Furfari, and F. Potortì, "Evaluating ambient assisted living solutions: The localization competition," *IEEE Pervasive Comput.*, vol. 12, no. 4, pp. 72–79, Oct./Dec. 2013.

[10] J. Morales and Z. Kassas, "Tightly-coupled inertial navigation system with signals of opportunity aiding," *IEEE Trans. Aerosp. Electron. Syst.*, vol. 57, no. 3, pp. 1930–1948, Jun. 2021.

[11] S. Beauregard, "A helmet-mounted pedestrian dead reckoning system," in *Proc. Int. Forum Appl. Wearable Comput.*, 2006, pp. 1–11.

[12] E. M. Diaz, "Inertial pocket navigation system: Unaided 3D positioning," *Sensors*, vol. 15, no. 4, pp. 9156–9178, 2015.

[13] E. Foxlin, "Pedestrian tracking with shoe-mounted inertial sensors," *IEEE Comput. Graph. Appl.*, vol. 25, no. 6, pp. 38–46, Nov. 2005.

[14] J.-O. Nilsson, A. K. Gupta, and P. Händel, "Foot-mounted inertial navigation made easy," in *Proc. Int. Conf. Indoor Positioning Indoor Navigat. (IPIN)*, Oct. 2014, pp. 24–29.

[15] A. R. Parrish, C.-S. Jao, and A. M. Shkel, "Stance phase detection for ZUPT-aided INS using knee-mounted IMU in crawling scenarios," *IEEE Sensors Lett.*, vol. 6, no. 5, pp. 1–4, May 2022.

[16] A. R. Jimenez, F. Seco, C. Prieto, and J. Guevara, "A comparison of pedestrian dead-reckoning algorithms using a low-cost MEMS IMU," in *Proc. IEEE Int. Symp. Intell. Signal Process.*, Aug. 2009, pp. 37–42.

[17] C.-S. Jao and A. M. Shkel, "ZUPT-aided INS bypassing stance phase detection by using foot-instability-based adaptive covariance," *IEEE Sensors J.*, vol. 21, no. 21, pp. 24338–24348, Nov. 2021.

[18] D. Titterton and J. Weston, *Strapdown Inertial Navigation Technology*, vol. 17, 2nd ed. London, U.K.: IET, 2004.

[19] Y. Wang, C.-S. Jao, and A. M. Shkel, "Scenario-dependent ZUPT-aided pedestrian inertial navigation with sensor fusion," *Gyroscopy Navigat.*, vol. 12, no. 1, pp. 1–16, Jan. 2021.

[20] Y. Wang, Y.-W. Lin, S. Askari, C.-S. Jao, and A. M. Shkel, "Compensation of systematic errors in ZUPT-aided pedestrian inertial navigation," in *Proc. IEEE/ION Position, Location Navigat. Symp. (PLANS)*, Apr. 2020, pp. 1452–1456.

[21] Y. Wang, A. Chernyshoff, and A. M. Shkel, "Error analysis of ZUPT-aided pedestrian inertial navigation," in *Proc. Int. Conf. Indoor Positioning Indoor Navigat. (IPIN)*, Sep. 2018, pp. 206–212.

[22] J. Wahlstrom and I. Skog, "Fifteen years of progress at zero velocity: A review," *IEEE Sensors J.*, vol. 21, no. 2, pp. 1139–1151, Jan. 2020.

[23] C.-S. Jao and A. M. Shkel, "A reconstruction filter for saturated accelerometer signals due to insufficient FSR in foot-mounted inertial navigation system," *IEEE Sensors J.*, vol. 22, no. 1, pp. 695–706, Jan. 2022.

[24] C.-S. Jao, Y. Wang, S. Askari, and A. M. Shkel, "A closed-form analytical estimation of vertical displacement error in pedestrian navigation," in *Proc. IEEE/ION Position, Location Navigat. Symp. (PLANS)*, Apr. 2020, pp. 793–797.

[25] C.-S. Jao, Y. Wang, Y.-W. Lin, and A. M. Shkel, "A hybrid barometric/ultrasonic altimeter for aiding ZUPT-based inertial pedestrian navigation systems," in *Proc. 33rd Int. Tech. Meeting Satell. Division Inst. Navigat. (ION GNSS)*, Oct. 2020, pp. 2500–2517.

[26] Q. Wang, Z. Guo, Z. Sun, X. Cui, and K. Liu, "Research on the forward and reverse calculation based on the adaptive zero-velocity interval adjustment for the foot-mounted inertial pedestrian-positioning system," *Sensors*, vol. 18, no. 5, p. 1642, May 2018.

[27] M. Laverne, M. George, D. Lord, A. Kelly, and T. Mukherjee, "Experimental validation of foot-to-foot range measurements in pedestrian tracking," in *Proc. ION GNSS*, 2011, pp. 1386–1393.

[28] Y. Wang, S. Askari, C.-S. Jao, and A. M. Shkel, "Directional ranging for enhanced performance of aided pedestrian inertial navigation," in *Proc. IEEE Int. Symp. Inertial Sensors Syst. (INERTIAL)*, Apr. 2019, pp. 1–2.

[29] C.-S. Jao, Y. Wang, and A. M. Shkel, "Pedestrian inertial navigation system augmented by vision-based foot-to-foot relative position measurements," in *Proc. IEEE/ION Position, Location Navigat. Symp. (PLANS)*, Apr. 2020, pp. 900–907.

[30] C.-S. Jao, Y. Wang, and A. M. Shkel, "A zero velocity detector for foot-mounted inertial navigation systems aided by downward-facing range sensor," in *Proc. IEEE SENSORS*, Oct. 2020, pp. 1–4.

[31] C.-S. Jao, A. Parrish, and A. M. Shkel, "'Sugar-cube' PLT: A real-time pedestrian localization testbed utilizing foot-mounted IMU/barometer/ultrasonic sensors," in *Proc. IEEE Sensors*, Oct. 2021, pp. 1–4.

[32] C.-S. Jao, K. Stewart, J. Conradt, E. Neftci, and A. M. Shkel, "Zero velocity detector for foot-mounted inertial navigation system assisted by a dynamic vision sensor," in *Proc. DGON Inertial Sensors Syst. (ISS)*, Sep. 2020, pp. 1–18.

[33] M. Ma, Q. Song, Y. Gu, Y. Li, and Z. Zhou, "An adaptive zero velocity detection algorithm based on multi-sensor fusion for a pedestrian navigation system," *Sensors*, vol. 18, no. 10, p. 3261, Sep. 2018.

[34] A. Norrdine, Z. Kasmi, and J. Blankenbach, "Step detection for ZUPT-aided inertial pedestrian navigation system using foot-mounted permanent magnet," *IEEE Sensors J.*, vol. 16, no. 17, pp. 6766–6773, Sep. 2016.

[35] J. Zhu and S. S. Kia, "Cooperative localization under limited connectivity," *IEEE Trans. Robot.*, vol. 35, no. 6, pp. 1523–1530, Dec. 2019.

[36] J. Zhu and S. S. Kia, "Decentralized cooperative localization with LoS and NLoS UWB inter-agent ranging," *IEEE Sensors J.*, vol. 22, no. 6, pp. 5447–5456, Mar. 2021.

[37] J.-O. Nilsson, D. Zachariah, I. Skog, and P. Händel, "Cooperative localization by dual foot-mounted inertial sensors and inter-agent ranging," *EURASIP J. Adv. Signal Process.*, vol. 2013, no. 1, pp. 1–17, Dec. 2013.

[38] A. A. Abdallah, C.-S. Jao, Z. M. Kassas, and A. M. Shkel, "A pedestrian indoor navigation system using deep-learning-aided cellular signals and ZUPT-aided foot-mounted IMUs," *IEEE Sensors J.*, vol. 22, no. 6, pp. 5188–5198, Mar. 2022.

[39] J. Zhu and S. S. Kia, "A loosely coupled cooperative localization augmentation to improve human geolocation in indoor environments," in *Proc. Int. Conf. Indoor Positioning Indoor Navigat. (IPIN)*, Sep. 2018, pp. 206–212.

[40] F. de Ponte Müller, "Survey on ranging sensors and cooperative techniques for relative positioning of vehicles," *Sensors*, vol. 17, no. 2, p. 271, 2017.

[41] Z. Kassas, *Position, Navigation, and Timing Technologies in the 21st Century*, vol. 2, J. Morton, F. van Diggelen, J. Spilker, Jr., and B. Parkinson, Eds. Hoboken, NJ, USA: Wiley, 2021, ch. 38, pp. 1171–1223.

[42] A. A. Abdallah, J. Khalife, and Z. M. Kassas, "Experimental characterization of received 5G signals carrier-to-noise ratio in indoor and urban environments," in *Proc. IEEE 93rd Veh. Technol. Conf. (VTC-Spring)*, Apr. 2021, pp. 1–5.

[43] A. Abdallah and Z. Kassas, "Multipath mitigation via synthetic aperture beamforming for indoor and deep urban navigation," *IEEE Trans. Veh. Technol.*, vol. 70, no. 9, pp. 8838–8853, Sep. 2021.

[44] Z. Kassas, J. Morales, K. Shamaei, and J. Khalife, "LTE steers UAV," *GPS World Mag.*, vol. 28, no. 4, pp. 18–25, Apr. 2017.

[45] M. Maaref and Z. M. Kassas, "Autonomous integrity monitoring for vehicular navigation with cellular signals of opportunity and an IMU," *IEEE Trans. Intell. Transp. Syst.*, vol. 23, no. 6, pp. 5586–5601, Jun. 2022.

[46] J. J. Morales, J. J. Khalife, and Z. M. Kassas, "Information fusion strategies for collaborative inertial radio SLAM," *IEEE Trans. Intell. Transp. Syst.*, early access, Nov. 8, 2021, doi: 10.1109/TITS.2021.3118678.

[47] I. Skog, P. Handel, J.-O. Nilsson, and J. Rantakokko, "Zero-velocity detection-an algorithm evaluation," *IEEE Trans. Biomed. Eng.*, vol. 57, no. 11, pp. 2657–2666, Nov. 2010.

[48] J. Zhu and S. S. Kia, "An UWB-based communication protocol design for an infrastructure-free cooperative navigation," in *Proc. IEEE/ION Position, Location Navigat. Symp. (PLANS)*, Apr. 2020, pp. 360–366.

[49] C. Chen, C.-S. Jao, A. M. Shkel, and S. S. Kia, "UWB sensor placement for foot-to-foot ranging in dual-foot-mounted ZUPT-aided INS," *IEEE Sensors Lett.*, vol. 6, no. 2, pp. 1–4, Feb. 2022.

[50] J. Morales and Z. M. Kassas, "Optimal collaborative mapping of terrestrial transmitters: Receiver placement and performance characterization," *IEEE Trans. Aerosp. Electron. Syst.*, vol. 54, no. 2, pp. 992–1007, Apr. 2018.

[51] A. A. Abdallah and Z. M. Kassas, "Deep learning-aided spatial discrimination for multipath mitigation," in *Proc. IEEE/ION Position, Location Navigat. Symp. (PLANS)*, Apr. 2020, pp. 1324–1335.

[52] E. Gökalp, O. Güngör, and Y. Boz, "Evaluation of different outlier detection methods for GPS networks," *Sensors*, vol. 8, no. 11, pp. 7344–7358, Nov. 2008.

[53] S. Askari, C.-S. Jao, Y. Wang, and A. M. Shkel, "A laboratory testbed for self-contained navigation," in *Proc. IEEE Int. Symp. Inertial Sensors Syst. (INERTIAL)*, Apr. 2019, pp. 1–2.

[54] J. Zhu and S. S. Kia, "Bias compensation for UWB ranging for pedestrian geolocation applications," *IEEE Sensors Lett.*, vol. 3, no. 9, pp. 1–4, Sep. 2019.

[55] J.-O. Nilsson, I. Skog, P. Händel, and K. V. S. Hari, "Foot-mounted INS for everybody—An open-source embedded implementation," in *Proc. IEEE/ION Position, Location Navigat. Symp.*, Apr. 2012, pp. 140–145.

[56] *NEON Personnel Tracker Pro*. Accessed: May 15, 2022. [Online]. Available: www.trxsystems.com

[57] Q. Yuan, I.-M. Chen, and A. Caus, "Human velocity tracking and localization using 3 IMU sensors," in *Proc. 6th IEEE Conf. Robot., Autom. Mechatronics (RAM)*, Nov. 2013, pp. 25–30.
[58] M. Angermann, P. Robertson, T. Kemptner, and M. Khider, "A high precision reference data set for pedestrian navigation using foot-mounted inertial sensors," in *Proc. Int. Conf. Indoor Positioning Indoor Navigat.*, Sep. 2010, pp. 1–6.

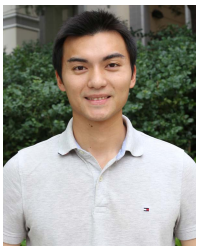

Chi-Shih Jao (Student Member, IEEE) received the B.S. degree in electrical engineering from the National Tsing Hua University, Hsinchu, Taiwan, in 2015, and the M.S. degree in electrical engineering from the Pennsylvania State University, University Park, PA, USA, in 2018. He is currently pursuing the Ph.D. degree with the Microsystems Laboratory, Department of Mechanical and Aerospace Engineering, University of California at Irvine. His research interests include inertial navigation by sensor fusion approach and vision-based inertial navigation. He was a recipient of the Holmes Fellowship from 2019 to 2020.

Ali A. Abdallah (Student Member, IEEE) is pursuing the Ph.D. degree with the Department of Electrical Engineering and Computer Science (EECS), University of California at Irvine and a member of the Autonomous Systems Perception, Intelligence, and Navigation (ASPIN) Laboratory. He was a recipient of the Best Student Paper Award from the 2020 IEEE/ION Position, Location, and Navigation Symposium (PLANS) and the Grand Prize from the 2020 IEEE Signal Processing Society video contest for beamforming research (5-MICC).

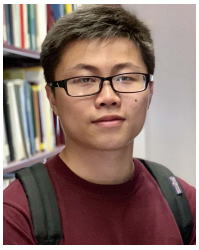

Changwei Chen received the B.S. degree from the Wuhan University of Technology, China, and the M.S. degree in mechanical and aerospace engineering from the University of California at Irvine, Irvine, CA, USA, where he is currently pursuing the Ph.D. degree with the Cooperative Systems Laboratory. His research interests include integrity monitoring algorithms for multi-sensor systems, cooperative navigation of multiple mobile agents, Kalman filtering, and sensor fusion. He was a recipient of the Holmes Fellowship from 2021 to 2022.

Min-Won Seo (Student Member, IEEE) is pursuing the Ph.D. degree with the Cooperative Systems Laboratory, Department of Mechanical and Aerospace Engineering, University of California at Irvine, Irvine, CA, USA. He was a Research Engineer at LIG Nex1 Company Ltd. (formerly known as LG Innotek), Gyeonggi-do, South Korea, from January 2015 to July 2020. His research interests include integrated sensing, perception, cooperative navigation of multi-agent systems, and their implementation.

Solmaz S. Kia (Senior Member, IEEE) received the B.Sc. and M.Sc. degrees in aerospace engineering from the Sharif University of Technology, Iran, in 2001 and 2004, respectively, and the Ph.D. degree in mechanical and aerospace engineering from the University of California, Irvine (UCI), Irvine, CA, USA, in 2009. She was a Senior Research Engineer at SySense Inc., El Segundo, CA, USA, from June 2009 to September 2010. She was a Postdoctoral Researcher with the Department of Mechanical and Aerospace Engineering, University of California San Diego and UCI. She is an Associate Professor of Mechanical and Aerospace Engineering at UCI. Her main research interests, in a broad sense, include distributed optimization/coordination/estimation, nonlinear control theory, and probabilistic robotics. She was a recipient of the UC President's Postdoctoral Fellowship from 2012 to 2014, an NSF CAREER Award in 2017, and the Best *IEEE Control Systems Magazine* Paper Award in 2021. Dr. Kia is an Associate Editor of the IEEE SENSORS LETTERS, IEEE OPEN JOURNAL OF CONTROL SYSTEMS, *Automatica* (journal of IFAC), and IEEE TRANSACTIONS ON CONTROL OF NETWORK SYSTEMS.

Zaher (Zak) M. Kassas (Senior Member, IEEE) received the B.E. degree in electrical engineering from Lebanese American University, the M.S. degree in electrical and computer engineering from The Ohio State University, and the M.S.E. degree in aerospace engineering and the Ph.D. degree in electrical and computer engineering from The University of Texas at Austin. He is an Associate Professor at the University of California, Irvine, and the Director of the Autonomous Systems Perception, Intelligence, and Navigation (ASPIN) Laboratory. He is also the Director of the U.S. Department of Transportation, Center for Automated Vehicles Research with Multimodal AssurEd Navigation (CARMEN), focusing on navigation resiliency and security of highly automated transportation systems. His research interests include cyber-physical systems, navigation systems, autonomous vehicles, and intelligent transportation systems. He was a recipient of the 2018 National Science Foundation (NSF) CAREER Award, the 2019 Office of Naval Research (ONR) Young Investigator Program (YIP) Award, the 2022 Air Force Office of Scientific Research (AFOSR) YIP Award, the 2018 IEEE Walter Fried Award, the 2018 Institute of Navigation (ION) Samuel Burka Award, and the 2019 ION Colonel Thomas Thurlow Award. He is a Senior Editor of the IEEE TRANSACTIONS ON INTELLIGENT VEHICLES and an Associate Editor of the IEEE TRANSACTIONS ON AEROSPACE AND ELECTRONIC SYSTEMS and the IEEE TRANSACTIONS ON INTELLIGENT TRANSPORTATION SYSTEMS.

Andrei M. Shkel (Fellow, IEEE) received the Diploma (Hons.) degree in mechanics and mathematics from Lomonosov's Moscow State University, Moscow, Russia, in 1991, and the Ph.D. degree in mechanical engineering from the University of Wisconsin–Madison, Madison, WI, USA, in 1997. In 2000, he joined as a Faculty Member with the University of California at Irvine, Irvine, CA, USA, where he is currently a Professor with the Department of Mechanical and Aerospace Engineering. He was the Program Manager of the Microsystems Technology Office, Defense Advanced Research Projects Agency (DARPA), Arlington, VA, USA, from 2009 to 2013. His professional interests, reflected over 300 publications and three books, include *Solid-State Sensors and Actuators*, *Micro-Electromechanical Systems-Based Neuroprosthetics*, *Sensor-Based Intelligence*, and *Control Theory*. He holds over 42 issued patents. His current research interests include design, manufacturing, and advanced control of high-precision micromachined gyroscopes and self-contained inertial navigation systems. He is a Fellow of the National Academy of Inventors (NAI). He was a recipient of the 2002 George E. Brown, Jr., Award, the 2005 NSF CAREER Award, the 2006 UCI HSSoE Best Faculty Research Award, the 2009 IEEE Sensors Council Technical Achievement Award, and the 2020 UCI HSSoE Innovator of the Year Award. In 2013, he received the Office of the Secretary of Defense Medal for Exceptional Public Service. He has served on a number of editorial boards, most recently, as an Editor for the IEEE/ASME JOURNAL OF MICROELECTROMECHANICAL SYSTEMS and the *Journal of Gyroscopy and Navigation* and the Founding Chair for the IEEE International Symposium on Inertial Sensors and Systems (INERTIAL). He was the President of the IEEE Sensors Council from 2020 to 2021.